International Journal of Modern Manufacturing Technologies
ISSN 2067–3604, Vol. XIV, No. 1 / 2022
https://doi.org/10.54684/ijmmt.2022.14.1.104

NUMERICAL AND EXPERIMENTAL INVESTIGATION ON EFFECT OF DESIGN FACTORS ON SHEAR PROPERTIES OF ADDITIVELY MANUFACTURED TETRA-ANTI-CHIRAL CELLULAR METAMATERIAL

Soham Teraiya, Swapnil Vyavahare, Shailendra Kumar

Department of Mechanical Engineering, Sardar Vallabhbhai National Institute of Technology, Surat-395007, India

Corresponding author: Shailendra Kumar, skbudhwar@med.svnit.ac.in

Abstract: This paper presents numerical and experimental investigation on the effect of design factors on mechanical properties of tetra-anti-chiral cellular metamaterial under shear loading. Two design factors namely cylinder radius and strut thickness, and three response characteristics including shear strength, modulus and specific energy absorption (SEA) of structure are considered in the present study. Finite element analysis (FEA) of CAD models of structures is performed using non-linear mechanical simulation. For experimentation, specimens are manufactured using material extrusion technique of additive manufacturing. A novel fixture is designed and manufactured for quick loading and unloading of structures for shear testing. It is observed that with decrease in cylinder radius, strength and modulus increases, but SEA decreases. However, all three responses increase with increase in strut thickness. Optimization of design factors is performed using grey relational analysis to maximize responses. Furthermore, predictive models of responses are developed using regression analysis.

Key words: design factors, mechanical properties, tetra-anti-chiral; cellular; metamaterial; shear loading; material extrusion.

1. INTRODUCTION

Cellular materials are extensively used in the field of aerospace, biomedical, automotive and architecture, because of their unique characteristics such as light weight, high strength, and high rigidity (Ashby and Gibson, 1997; Ashby, 2006; Bălţătescu et al., 2013). Cellular materials with negative Poisson's ratio are called metamaterials or auxetics. Geometry of such materials of structures are designed such that they contract laterally under the application of longitudinal compression load (Lakes, 1987). These structures have unique physical characteristics such as good indentation resistance, shear resistance, synclastic curvature, and other vibro-acoustic properties (Alderson and Alderson, 2007). Tetra-anti-chiral structure is one of the unique auxetic cellular structures that exhibits negative Poisson's ratio due to asymmetric rotational geometrical configuration. This structure has superior mechanical properties than other cellular auxetic structures (Alderson et al., 2010). The structure has three design factors namely cylinder radius (r), strut thickness (t) and strut length (L) as depicted in Figure 1. Chiral structures are recently used in various applications such as biomedical stents, airfoil morphing, turbine dampers, and sports helmets(Bornengo et al., 2005; Agnese et al., 2015; Duncan et al., 2018; Geng et al., 2019; Bai et al., 2021). As these structures have complex geometrical configurations, conventional manufacturing processes are generally not used for their fabrication. Material extrusion is one of the technique of additive manufacturing (AM) widely used to fabricate complex structures (Singh and Pandey, 2015). In this process, feedstock materials such as acrylonitrile butadiene styrene (ABS), polylactic acid (PLA), polyethylene terephthalate glycol (PETG), and high impact polystyrene (HIPS) is used in the form of filament to fabricate parts directly from CAD models (Cotoros and Baritz, 2012; Ciofu et al., 2018).

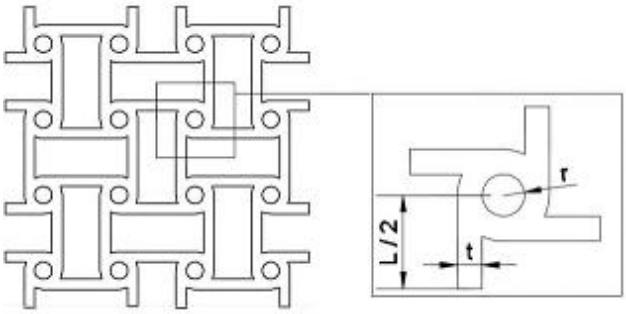

Fig. 1. Unit cell of tetra-anti-chiral metamaterial

Various researchers have investigated the mechanical performance of metamaterials under compressive, shear, and flexural loading. For example, Sugimura (2004) investigated the effect of design factors on shear strength and shear modulus of tetrahedral cellular sandwich structures and concluded that the strength of structure proportionately varies with relative density.

Pan et al. (2006) used computational and experimental methods to measure longitudinal shear strength of honeycomb structure and observed that the structure deforms in four stages i.e. elastic, plastic, fracture in the connection of the cell walls, and the debonding of a core with face sheets. Lira et al. (2009) performed numerical and computational investigation on out-of-plane shear properties of center-symmetric auxetic structures and found that the shear stiffness ratio increases with decrease in ligament length ratio. Lorato et al. (2010) compared the shear performance of various chiral and anti-chiral honeycombs. They reported that shear properties of all chiral structures are significantly influenced by cell wall aspect ratio and relative density of the structures. Chen et al. (2013) observed that shear modulus of the structure decreases with increase in ratio of ligament length and node radius. Fu et al. (2016) reported that the shear modulus of auxetic structure decreases with increase in cell wall-length ratio. Jin et al. (2019) investigated the effect of cell geometry and rotational rigidity of cylinders on shear resistance of chiral structures using picture frame apparatus. They found that overall stiffness ratio of the structure is greatly influenced by the materials of center joints. Henyš et al. (2019) used homogenization approach to conclude that the shear modulus is non-linearly dependent on geometric parameters of the structure. Novak et al. (2020) performed an experimental investigation to study the effect of porosity on mechanical properties of chiral sinusoidal honeycomb under shear and compressive loading. They used loading bars and fasteners for development of fixture for shear testing. The specimen was connected with the clamping plates using epoxy resin (adhesive). It was reported that the struts experience localized shear and tensile stresses during deformation of the structure. Bai et al. (2021) developed computational models for tensile and shear properties of chiral structure and reported that the mechanical properties of structure are ideal for morphing applications.

As shear properties of the auxetic structures are superior to conventional cellular structures, these structures have the potential to be widely used as a core in lightweight sandwich panels. Some researchers have theoretically investigated the effect of design factors on mechanical properties of structure under tensile, compression and flexural loading (Alderson et al., 2010; Lorato et al., 2010; Chen et al., 2013; Mousanezhad et al., 2016). However, very less literature is available on experimental work focused on studying the effect of design factors on shear properties of tetra-anti-chiral structures. Further, some researchers have performed shear testing of cellular structures using a conventional fixture having fasteners and adhesives (Aboura et al., 2004; Azzouz et al., 2019; Novak et al., 2020; Casavola et al., 2021). Loading and unloading of the specimen in these fixtures is time-consuming. Therefore, in the present work, efforts have been made to fulfill the above research gaps. A numerical and experimental investigation is performed to study the effect of design factors on response characteristics namely shear strength, shear modulus, and specific energy absorption (SEA) of the tetra-anti-chiral structures. A novel 'fit' based fixture (without fasteners and adhesives) is developed for quick loading and unloading of specimen. Experimental plan is prepared using face-centered central composite design. Specimens are fabricated using material extrusion technique and shear testing is performed on universal testing machine. Experimental results are analyzed using "analysis of variance" (ANOVA). Further, optimization of design factors is performed using grey relational analysis (GRA) to maximize the responses. Also, rgression models are developed to predict the response characteristics.

2. MATERIALS AND METHODS

A 2D model of the specimen of tetra-anti-chiral structure is shown in Figure 2(a). As volume fraction significantly affects the mechanical properties of the structures, therefore to compare mechanical performance of the structures under shear loading, the volume fraction of unit cell of all specimens is kept constant at 35% (Ashby and Gibson, 1997) . Volume fraction of the structure can be determined using Equation 1 (Lorato et al., 2010). In the current study, effect of design factors namely, cylinder radius (r) and strut thickness (t) on mechanical properties under shear loading is investigated. Strut length (L) is calculated using equation (1) for each specimen.

$$\rho/\rho_s = [\beta\{2\alpha+\pi(2-\beta)\}-2\{\emptyset-(1-\beta)\sin\emptyset\}]/\alpha^2 \quad (1)$$

Where, ρ_s= Density of solid, α= L/r, β = t/r, $\emptyset$=acos(1-β)

Size of the structure is decided according to American society for testing materials (ASTM) C273 standards. The 3D CAD model of the specimen for shear testing is developed using AutoCAD 2022 (Autodesk Inc) as shown in Figure 2(b).

Experimental plan is prepared using central composite design method of response surface methodology. Table 1 lists levels of design factors for experimental study. Experimental plan suggests a total of 22 specimens to be manufactured as listed in Table 2.

In present study, FEA of tetra-anti-chiral structure is performed using Abaqus/explicit V6.14 software. Meshing of the model is done using C3D8R hex-dominated elements. ACIS model of each configuration of structure is imported in Abaqus software. Non-linear material model is developed by compression testing of ASTM D695 standard sized ABS specimens.

Table 1. Design factor with range

Design Factor	-1 Level	0 Level	+1 Level
Cylinder Radius ‘r’ (mm)	0.25	0.5	0.75
Strut Thickness ‘t’ (mm)	0.8	1	1.2

Table 2. Experimental plan for shear testing of tetra-anti-chiral structures

Run No	Cylinder Radius ‘r’ (mm)	Strut Thickness ‘t’ (mm)	Configuration No
1	0.25	0.8	1
2	0.25	1	2
3	0.25	1.2	3
4	0.5	0.8	4
5	0.5	1	5
6	0.5	1.2	6
7	0.75	0.8	7
8	0.75	1	8
9	0.75	1.2	9
10	0.25	0.8	1
11	0.25	1	2
12	0.25	1.2	3
13	0.5	0.8	4
14	0.5	1	5
15	0.5	1.2	6
16	0.75	0.8	7
17	0.75	1	8
18	0.75	1.2	9
19	0.5	1	5
20	0.5	1	5
21	0.5	1	5
22	0.5	1	5

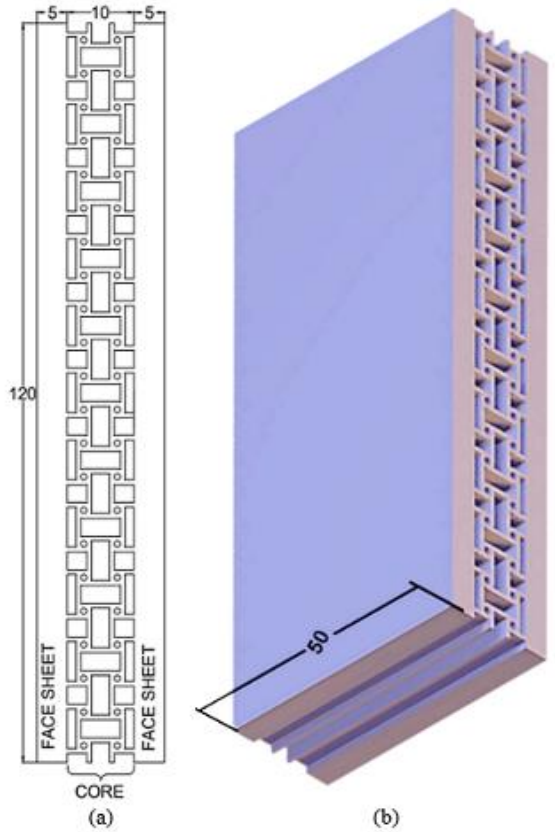

Fig. 2. (a) 2D CAD model and (b) 3D CAD model of tetra-anti-chiral metamaterial

Figure 3 shows load-displacement curves of two ABS specimens. From these curves, true stress and plastic strain of the material are determined, which are assigned to the FEA model. Table 3 lists non-linear mechanical properties of ABS material. As shown in Figure 4, mesh sensitivity analysis is performed with element size of 0.4, 0.8, and 1.2 mm. It is observed that results are converged for models with an element size of 0.4 mm. Thus, FEA models of all configurations are developed using a mesh size of 0.4 mm. In order to assess the effect of loading velocity on FEA results, multiple simulations are performed at 0.01, 0.1, and 1 mm/s. It is observed that FEA results are less sensitive to the loading velocities (Alomarah et al., 2020). Hence, each FEA model is assigned boundary conditions by giving displacement to the right face sheet of the specimen at the rate of 1.00 mm/s. Left face sheet of the model is fixed by giving ‘encastered’ boundary condition, which means that the face sheet will not move in any rotational and translational direction. The penalty-type tangential friction coefficient is kept at 0.1.

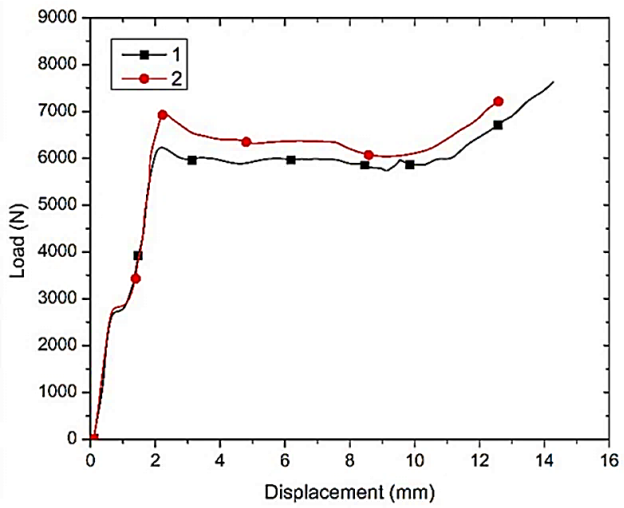

Fig. 3. Load-displacement curve of two ABS specimen for non-linear material model

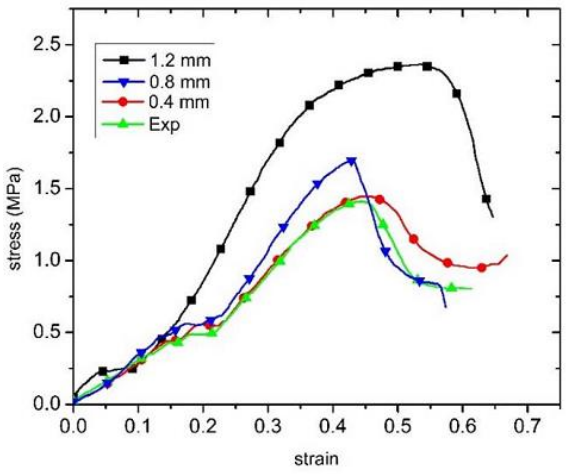

Fig. 4. Effect of element size of meshed model on FEA

Table 3. Non-linear mechanical properties of ABS material for FEA

Elastic Properties								
Young's Modulus (MPa)			Poisson's Ratio (Ingrole et al., 2017)			Density (kg/m^3)		
800			0.35			1210		
Plastic properties								
Plastic Strain	0	0.02	0.04	0.09	0.12	0.17	0.22	0.28
Plastic Stress (MPa)	23.26	27.15	56.4	58.69	59.74	63.01	67.65	68.59

For interaction, "All-with-self" type general contact is given to the whole model to avoid penetration of the deformed struts into each other. Total of nine set of FEA models are generated according to configurations listed in Table 2. Load-displacement values for all configuration are recorded from the "History output" of the analyzed results.

Further, as per the experimental plan, 22 specimens of ABS material are manufactured using a material extrusion machine (Model- Delta 2040, M/s Wasp, Italy). This machine has cylindrical build volume of Ø200×400 mm^3, with layer resolution of 50 µm. Also, machine has positional accuracy of 10 µm in X and Y direction. Nozzle diameter is 0.4 mm and maximum achievable print temperature is 260 ^{0}C. Maximum print speed of machine is 500 mm/s. Table 4 lists process parameters that are kept constant during fabrication of specimens.

Table 4. Constant process parameters of material extrusion

Parameter	Value
Build orientation	Flat (Unit cell in XY plane)
Print Temperature	240 °C
Bed Temperature	100 °C
Layer height	0.2 mm
Raster angle	0°
Print speed	40 mm/s
No of contour	01
Infill	100%

All manufactured specimens are tested under shear loading using a universal testing machine. A novel fixture is designed and fabricated for quick loading and unloading of structures for shear testing. The CAD model and actual photograph of fixture with the loaded specimen is shown in Figure 5. This fixture is an assembly of a holding component and two shear plates. As shown in Figure 5(b), left shear plate remains stationary and holds specimen, while right shear plate applies the load on specimen. From the shear tests, load-displacement values are recorded and, response characteristics namely shear strength (τ), shear modulus (G), and SEA are determined. Shear strength (τ) is a ratio of maximum shear load taken by a core of specimen and original surface area (equation (2)). Shear modulus (G) and SEA are determined using equation (3) and (4).

$$\tau = P_{max} / A_s \quad (2)$$

$$G = [(\Delta P/\Delta u) \times c] / (L \times b) \quad (3)$$

$$SEA = \left({}_0\int^{\gamma} \tau(\gamma)\, d\gamma\right)/\rho \quad (4)$$

Where, τ = Shear strength (MPa), P_{max} = Maximum shear load taken by the structure (N), A_s = Surface area (mm^2) = (L×b), c = Core thickness (mm), L= Length of the specimen (mm), b = Width of the specimen (mm), $(\Delta P/\Delta u) = (P_b-P_a)/(u_b-u_a)$ = Slope of the initial linear portion of load-displacement curve (N/mm), γ = Shear strain, ρ = Density of the structure (g/mm^3)

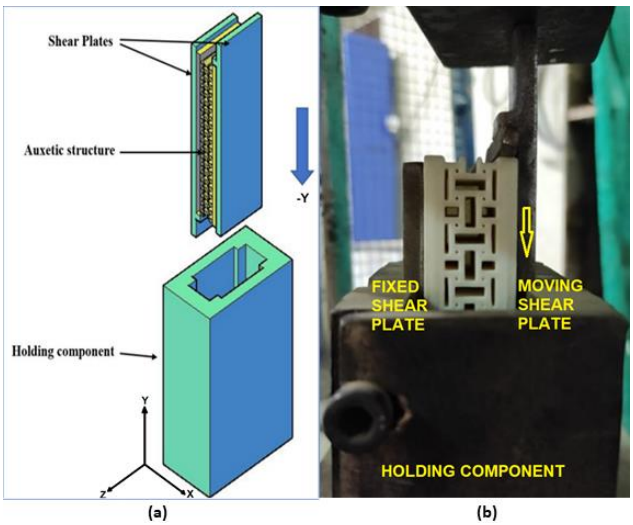

Fig. 5. (a) 3D CAD model of the novel fixture, (b) Actual photograph of fixture for shear testing of structure

3. RESULTS AND DISCUSSION

Typical load-displacement curve recorded during FEA and experimental investigation is shown in Figure 6(a). Enlarged image of deformed structure and deformation sequence of specimen at each critical point of the load-displacement curve are depicted in Figure 6(b) and 6(c) respectively. During shear testing, left face sheet is fixed in the shear plate of fixture and load is applied on the right face sheet of specimen. On applying load, initially elastic deformation of structure occurs till 1.1 mm. Upon further loading, structure starts to deform plastically. The cylinders of unit cell rotate due to development of torque along their circumferences. Also, normal forces apply in a negative Y-direction along the center of the cylinder that tries to buckle struts.

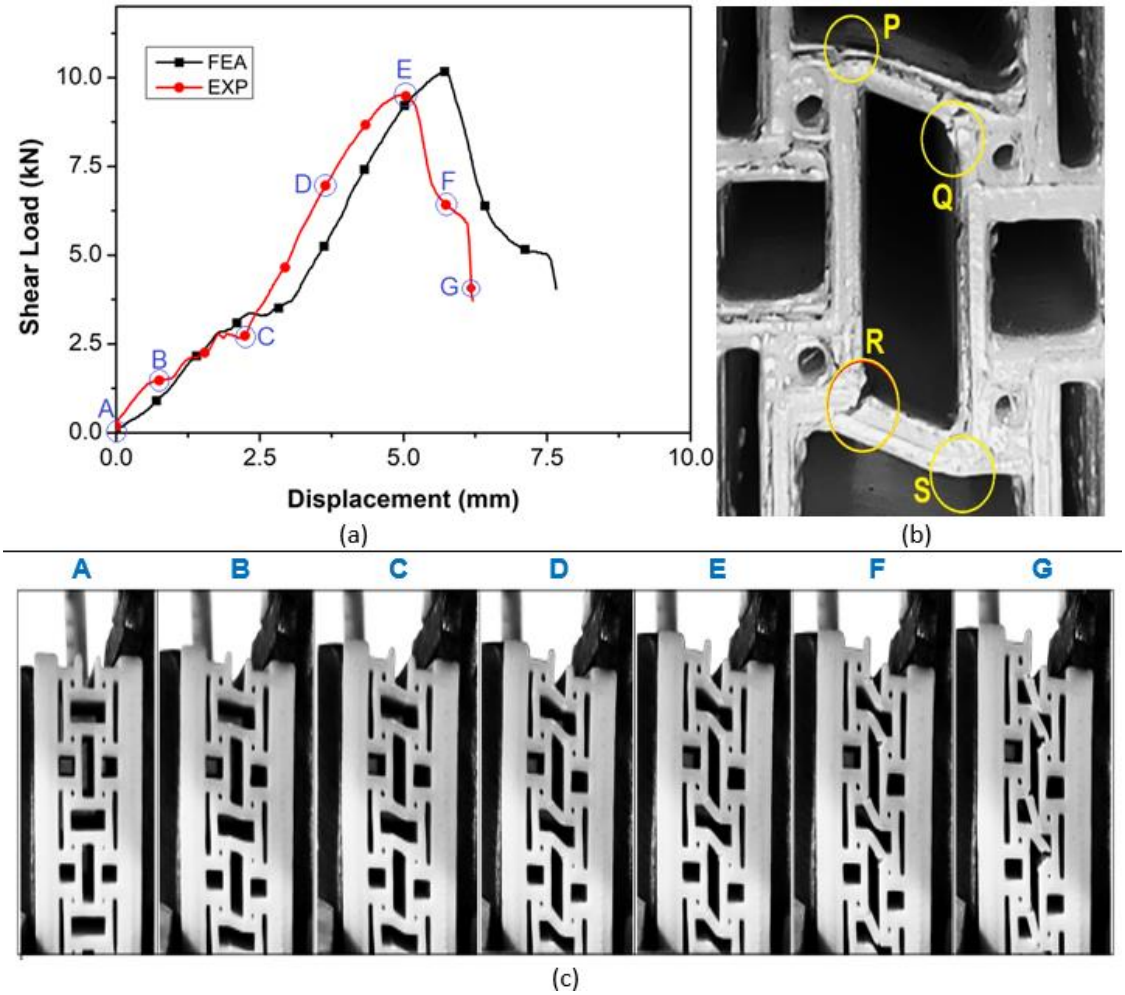

Fig. 6. (a) Typical load-displacement curve recorded during FEA and experimental investigation, (b) Enlarged image of deformed unit cell of the structure, (c) Deformation sequence of the specimen at critical points of load-displacement graph

Due to rotation of the cylinder, it pulls struts towards center. As a result, buckling forces and torque work against each other in vertical struts. This effect is not observed in horizontal struts due to absence of vertical normal buckling load. Horizontal struts experience only tensile stresses developed due to torque generation around rotating cylinders. Stresses in vertical strut are less as compared to the horizontal struts and joints. At a displacement of 2 mm, tensile stresses are generated in regions P and S as depicted in Figure 6(b). With further increase in load (at 2.5 mm displacement), local shear deformation is observed at regions Q and R, which are located at the junction of strut and cylinders of each unit cell. Simultaneously, local tensile deformation is observed in region P and S. Load-displacement values increase non-linearly up to 8.75 kN load and finally, crack appears in regions Q and R at 9.375 kN load. Thereafter, the ability of a structure to bear further load starts decreasing. As the crack propagates further, the load values decrease with increase in displacement. At 5.9 kN load, complete shear fracture is observed in the unit cell of the structure in the region Q and R. Similar trend is observed in the stress-strain curve of all tested specimens. From Figure 6(b), it is observed that the direction of crack propagation is not linear but tangential to the adjacent cylinders. It happens due to development of stress concentration zones created around the junction of cylinders and struts. Also, upon critical observation, it is found that slicing software and machine have limitations to print material at intricate areas of the structure; which create porosities. During local shear in the region, Q and R, the crack propagates through these porosities, which are tangentially aligned to the internal diameter of the cylinder. Due to the presence of micro-voids and porosities in fabricated specimens, structure deforms earlier during shear testing as compared to FEA. Table 5 lists the experimental results of shear testing of tetra-anti-chiral structure using novel fixture. ANOVA is performed on experimental results as given in Table 6. It is observed that both the design factors namely cylinder radius and strut thickness, significantly affect all response characteristics such as strength (τ), modulus (G), and SEA.

Table 5. Experimental results for shear testing of tetra-anti-chiral structures

	Factor 1	Factor 2	Response 1	Response 2	Response 3
Run	Cylinder radius 'r' (mm)	Strut thickness 't' (mm)	Strength (MPa)	Modulus (MPa)	SEA (J/gm)
1	0.25	0.8	1.850	1.875	0.551
2	0.25	1	2.040	3.046	1.013
3	0.25	1.2	2.613	3.476	1.382
4	0.5	0.8	1.580	1.746	0.865
5	0.5	1	1.720	2.720	1.292
6	0.5	1.2	2.265	3.032	1.698
7	0.75	0.8	1.585	1.452	0.822
8	0.75	1	1.685	2.316	1.391
9	0.75	1.2	2.140	2.292	1.756
10	0.25	0.8	1.810	1.997	0.628
11	0.25	1	2.010	3.109	1.042
12	0.25	1.2	2.700	3.546	1.412
13	0.5	0.8	1.590	1.676	0.943
14	0.5	1	1.700	2.747	1.352
15	0.5	1.2	2.200	2.974	1.799
16	0.75	0.8	1.620	1.594	0.925
17	0.75	1	1.570	2.292	1.332
18	0.75	1.2	2.190	2.490	1.836
19	0.5	1	1.730	2.529	1.319
20	0.5	1	1.710	2.747	1.411
21	0.5	1	1.730	2.774	1.349
22	0.5	1	1.690	2.665	1.452

Table 6. ANOVA table for Shear Strength, modulus and SEA

Responses	Source	F-value	p-value
Shear Strength	A-r	307.07	< 0.05
	B-t	1021.61	< 0.05
Shear Modulus	A-r	315.48	< 0.05
	B-t	827.05	< 0.05
SEA	A-r	137.16	< 0.05
	B-t	880.11	< 0.05

Table 7. Predictive models for influence of design factors on shear properties of the structure

Strength = 5.695 - 1.583×r - 8.514×t - 1.32×r×t + 2.158×r² + 5.435×t²
Modulus = -10.096 + 2.190×r + 22.153×t + -3.533×r×t - 0.194×r² - 8.636×t²
SEA = -2.326 + 2.739×r + 3.521×t + 0.575×r×t - 2.637×r² - 0.831×t²

It is observed that strength and modulus increase with decrease in cylinder radius and increase in strut thickness as depicted in Figure 7 and 8 respectively. As cylinder radius decreases, eccentricity between a line of action of load for two consecutive unit cells decreases. Due to this, low torque is generated around the cylinders, which results in lesser local flexural and buckling stresses in struts. It increases the ability of a structure to resist plastic deformation under higher shear loads; and it results in increase in shear strength and modulus. At higher strut thickness, the effective area of structure under the applied load increases. It increases the ability of structure to bear the load without plastic deformation. Similar results are reported by Nečemer et al. (2020) on the basis of numerical investigation of chiral structures. Also, the area of tangential connection between the cylinder and strut is higher for t=1.2 mm than t = 0.8 mm. Thus, a higher load is required to rotate the cylinders. It increases shear strength and shear modulus of structure. It is observed that on varying the strut thickness from 0.8 mm to 1.2 mm, shear strength is increased by 44.81% and 34.59% with cylinder radius of 0.25 mm and 0.75 mm respectively. It means that the interaction effect of design factors is significant for shear strength of the structure. In aerospace domain, fuselage of the aircraft experiences high shear loads (Megson, 2013). Sandwich panels with regular hexagonal honeycomb cores have less shear resistance as compared to tetra-anti-chiral auxetic structures (Ashby and Gibson, 1997). Therefore, in these parts, core of the sandwich panel can be made of the tetra-anti-chiral structure, which has a lower cylinder radius and higher strut thickness.

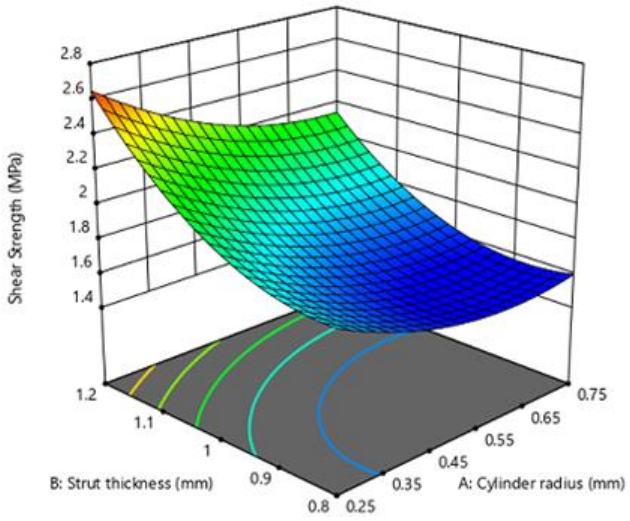

Fig. 7. Effect of design factors on shear strength

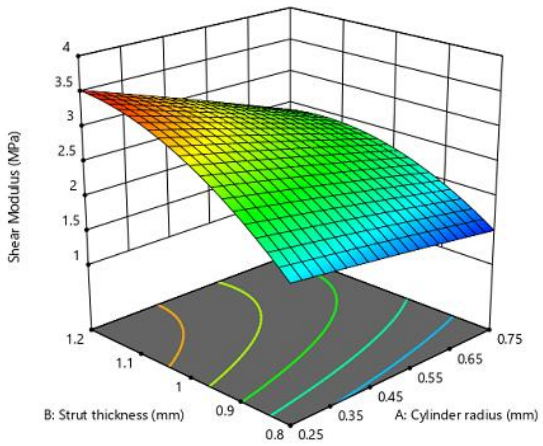

Fig. 8. Effect of design factors on shear modulus

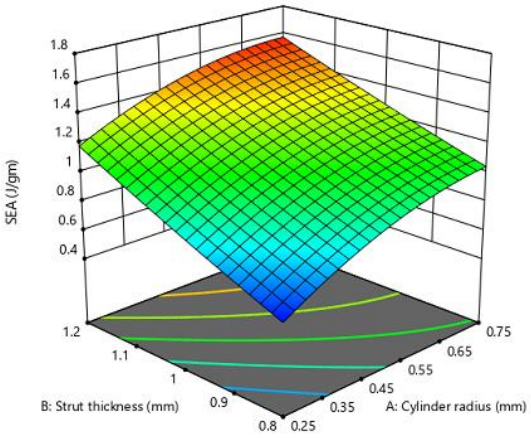

Fig. 9. Effect of design factors on SEA

It is observed that SEA of tetra-anti-chiral structure increases with increase in cylinder radius and strut thickness of unit cells as depicted in Figure 9. With increase in cylinder radius, the eccentricity of applied load increases. It reduces direct load on the successive cylinder of the unit cell. Also, due to rotation of unit cell, higher strain is observed for the structure during loading. Therefore, the structure takes a uniform load up to higher strain values. Due to this phenomenon, the area under the stress-strain curve increases, and thus SEA of structure increases. Also, with increase in strut thickness, the ability of structure to bear load increases; which results in increase in SEA. In aerospace industries, energy absorption for airfoil morphing is a major concern. Therefore, in airfoil morphing components, tetra-anti-chiral structure with higher cylinder radius and strut thickness should be used (Airoldi et al., 2015).

Based on experimental results, predictive models (Table 7) are developed using regression analysis for shear strength, shear modulus, and SEA of tetra-anti-chiral structures. From Table 8, the results of experimental tests and FEA are found to be in good agreement with each other. Experimental results are further validated using confirmation tests performed by taking random levels of design factors. The results of the confirmation test are consistent with experimental results (Table 9).

Further, to maximize response characteristics, optimization of design factors is performed using GRA technique. Using experimental results, normalization of response, deviation sequence, grey relational gradient, and ranking of GRA are determined. The structure which has the best ranking is designated as optimum configuration. From Table 10, it is observed that the unit cell with configuration 3 (Run 3, 12) having design parameters r = 0.25, t=1.2 is optimum.

Table 8. Comparison of experimental and FEA results

r (mm)	t (mm)	Strength (MPa)			Modulus (MPa)			SEA (J/gm)		
		Experimental	FEA	(%) Deviation	Experimental	FEA	(%) Deviation	Experimental	FEA	(%) Deviation
0.25	1	2.04	1.94	4.95	3.05	2.99	1.78	1.01	1.00	1.28
0.25	1.2	2.613	2.68	-2.54	3.48	3.38	2.70	1.38	1.28	7.64
0.5	0.8	1.58	1.57	0.36	1.75	1.63	6.38	0.87	0.96	-10.67
0.5	1	1.72	1.55	9.90	2.72	2.88	-5.74	1.29	1.15	10.92
0.75	1.2	2.14	2.24	-4.67	2.29	2.48	-8.24	1.76	1.73	1.61

Table 9. Results of confirmation tests conducted at randomized levels of design factors

r (mm)	t (mm)	Strength (MPa)			Modulus (MPa)			SEA (J/gm)		
		Predicted	Observed	(%) Deviation	Predicted	Observed	(%) Deviation	Predicted	Observed	(%) Deviation
0.25	1	2.026	1.888	-6.770	3.072	3.203	4.29	1.027	1.123	9.360
0.5	1.2	2.261	2.340	3.48	2.976	2.752	-7.550	1.757	1.884	7.240
0.75	0.8	1.597	1.525	-4.530	1.511	1.659	9.74	0.875	0.780	-10.790
0.25	0.8	1.838	1.951	6.17	1.927	1.768	-8.250	0.594	0.639	7.69
0.5	1	1.705	1.782	4.550	2.699	2.881	6.74	1.361	1.286	-5.520

Table 10. Optimization using GRA for shear properties of tetra-anti-chiral auxetic structures

	NORMALIZED VALUES			DEVIATION SEQUENCE			GREY RELATIONAL COEEFICIENT			GRADE	RANK
Run	**Strength**	**Modulus**	**SEA**	**Strength**	**Modulus**	**SEA**	**Strength**	**Modulus**	**SEA**		
1	0.248	0.202	0.020	0.752	0.798	0.980	0.444	0.429	0.380	0.313	21
2	0.416	0.761	0.317	0.584	0.239	0.683	0.507	0.715	0.468	0.422	8
3	**0.923**	**0.966**	**0.572**	**0.077**	**0.034**	**0.428**	**0.886**	**0.947**	**0.584**	**0.604**	**2**
4	0.009	0.141	0.347	0.991	0.859	0.653	0.377	0.411	0.479	0.317	19
5	0.133	0.606	0.578	0.867	0.394	0.422	0.409	0.603	0.587	0.400	11
6	0.615	0.755	0.878	0.385	0.245	0.122	0.609	0.710	0.831	0.537	3
7	0.013	0.000	0.522	0.987	1.000	0.478	0.378	0.375	0.556	0.327	17
8	0.102	0.412	0.709	0.898	0.588	0.291	0.400	0.505	0.674	0.395	14
9	0.504	0.401	1.000	0.496	0.599	0.000	0.548	0.501	1.000	0.512	5
10	0.212	0.260	0.000	0.788	0.740	1.000	0.432	0.448	0.375	0.314	20
11	0.389	0.791	0.278	0.611	0.209	0.722	0.496	0.742	0.454	0.423	7
12	**1.000**	**1.000**	**0.626**	**0.000**	**0.000**	**0.374**	**1.000**	**1.000**	**0.616**	**0.654**	**1**
13	0.018	0.107	0.306	0.982	0.893	0.694	0.379	0.402	0.464	0.311	22
14	0.115	0.619	0.599	0.885	0.381	0.401	0.404	0.611	0.600	0.404	10
15	0.558	0.727	0.878	0.442	0.273	0.122	0.576	0.687	0.831	0.523	4
16	0.044	0.068	0.433	0.956	0.932	0.567	0.386	0.392	0.514	0.323	18
17	0.000	0.401	0.697	1.000	0.599	0.303	0.375	0.500	0.665	0.385	16
18	0.549	0.496	0.927	0.451	0.504	0.073	0.571	0.543	0.892	0.501	6
19	0.142	0.515	0.643	0.858	0.485	0.357	0.411	0.553	0.627	0.398	12
20	0.124	0.619	0.534	0.876	0.381	0.466	0.406	0.611	0.563	0.395	13
21	0.142	0.631	0.621	0.858	0.369	0.379	0.411	0.620	0.613	0.411	9
22	0.106	0.580	0.556	0.894	0.420	0.444	0.402	0.588	0.575	0.391	15

4. CONCLUSION

Numerical and experimental investigation has been performed to study the effect of design factors on mechanical properties of the tetra-anti-chiral cellular metamaterial under shear loading. Shear testing of fabricated specimens has been done using a novel 'fit' based fixture for quick loading and unloading. It is found that strength and modulus increase with decrease in cylinder radius and increase in strut thickness. SEA of tetra-anti-chiral structure increases with increase in cylinder radius and strut thickness of unit cells of structure. Regression models have been developed to predict the responses. Confirmation tests have also been performed at random levels of design factors to validate the experimental results and predictive models. Further, optimization of design factors has been performed to maximize response characteristics. Findings of the present study will be helpful in designing the tetra-anti-chiral cellular structures for the core of sandwich panels to achieve desirable shear properties in aerospace, automotive, biomedical, sports and packaging industries.

5. REFERENCES

1. Aboura, Z., Talbi, N., Allaoui, S., Benzeggagh, M., (2004). *Elastic behavior of corrugated cardboard: experiments and modeling*, Compos. Struct., **63,** 53-62.

2. Agnese, F., Remillat, C., Scarpa, F., Payne, C., (2015). *Composite chiral shear vibration damper*, Compos. Struct., **132,** 215-225.

3. Airoldi, A., Bettini, P., Panichelli, P., Oktem, M. F., Sala, G., (2015). *Chiral topologies for composite morphing structures–Part I: Development of a chiral rib for deformable airfoils*, Phys. Status Solidi B, **252,** 1435-1445.

4. Alderson, A., Alderson, K., (2007). *Auxetic materials*, Proc. Inst. Mech. Eng., Part G, **221,** 565-575.

5. Alderson, A., Alderson, K. L., Attard, D., Evans, K. E., Gatt, R., Grima, J. N., Miller, W., Ravirala, N., Smith, C., Zied, K., (2010). *Elastic constants of 3-, 4- and 6-connected chiral and anti-chiral honeycombs subject to uniaxial in-plane loading*, Compos. Sci. Technol., **70,** 1042-1048.

6. Alomarah, A., Masood, S. H., Sbarski, I., Faisal, B., Gao, Z., Ruan, D., (2020). *Compressive properties of 3D printed auxetic structures: experimental and numerical studies*, Virtual and Physical Prototyping, **15,** 1-21.

7. Ashby, M. F., (2006). *The properties of foams and lattices*, Philos. Trans. R. Soc., A, **364,** 15-30.

8. Ashby, M. F., Gibson, L. J., (1997). *Cellular solids: structure and properties*, Press Syndicate of the University of Cambridge, Cambridge, UK, 175-231.

9. Azzouz, L., Chen, Y., Zarrelli, M., Pearce, J. M., Mitchell, L., Ren, G., Grasso, M., (2019). *Mechanical*

properties of 3-D printed truss-like lattice biopolymer non-stochastic structures for sandwich panels with natural fibre composite skins, Compos. Struct., **213,** 220-230.
10. Bai, Y., Zhao, T., Yuan, C., Liu, W., Zhang, H., Yang, L., She, C., (2021). *Mechanical Properties of a Chiral Cellular Structure with Semicircular Beams*, Mater., **14,** 2887.
11. Bălţătescu, O., Florea, R. M., Buzăianu, A., Roman, C., Carcea, I., (2013). *Manufacturing and characterization of stabilized aluminum foams*, Int. J. of Mod. Manufact. Technol., **1,** 17-24.
12. Bornengo, D., Scarpa, F., Remillat, C., (2005). *Evaluation of hexagonal chiral structure for morphing airfoil concept*, Proc. Inst. Mech. Eng., Part G, **219,** 185-192.
13. Casavola, C., Del Core, L., Moramarco, V., Pappalettera, G., Patronelli, M., (2021). *Full-field mechanical characterization of polyurethane foams under large deformations by digital image correlation*, Mech. Adv. Mater. Struct., 1-16.
14. Chen, Y., Scarpa, F., Liu, Y., Leng, J., (2013). *Elasticity of anti-tetrachiral anisotropic lattices*, Int. J. Solids Struct., **50,** 996-1004.
15. Ciofu, C., Carausu, C., Mazurchevici, S. N., Paunoiu, V., Chirita, B., (2018). *Equipment for testing the worm and worm gear assembly from" liquid wood" and comparative MEF analyses*, Int. J. of Mod. Manufact. Technol., **X**(2)**,** 45-50.
16. Cotoros, D., Baritz, M., (2012). *Implementing rapid prototyping technologies for corrective insoles*, Int. J. of Mod. Manufact. Technol., **4,** 41-46.
17. Duncan, O., Shepherd, T., Moroney, C., Foster, L., Venkatraman, P. D., Winwood, K., Allen, T., Alderson, A., (2018). *Review of auxetic materials for sports applications: Expanding options in comfort and protection*, Appl. Sci., **8,** 941.
18. Fu, M., Xu, O., Hu, L., Yu, T., (2016). *Nonlinear shear modulus of re-entrant hexagonal honeycombs under large deformation*, Int. J. Solids Struct., **80,** 284-296.
19. Geng, L., Ruan, X., Wu, W., Xia, R., Fang, D., (2019). *Mechanical properties of selective laser sintering (SLS) additive manufactured chiral Auxetic cylindrical stent*, Exp. Mech., **59,** 913-925.
20. Henyš, P., Vomáčko, V., Ackermann, M., Sobotka, J., Solfronk, P., Šafka, J., Čapek, L., (2019). *Normal and shear behaviours of the auxetic metamaterials: homogenisation and experimental approaches*, Meccanica, **54,** 831-839.
21. Ingrole, A., Hao, A., Liang, R., (2017). *Design and modeling of auxetic and hybrid honeycomb structures for in-plane property enhancement*, Mater. Des., **117,** 72-83.
22. Jin, S., Korkolis, Y. P., Li, Y., (2019). *Shear resistance of an auxetic chiral mechanical metamaterial*, Int. J. Solids Struct., **174,** 28-37.
23. Lakes, R., (1987). *Foam structures with a negative Poisson's ratio*, Science, **235,** 1038-1041.
24. Lira, C., Innocenti, P., Scarpa, F., (2009). *Transverse elastic shear of auxetic multi re-entrant honeycombs*, Compos. Struct., **90,** 314-322.
25. Lorato, A., Innocenti, P., Scarpa, F., Alderson, A., Alderson, K., Zied, K., Ravirala, N., Miller, W., Smith, C., Evans, K., (2010). *The transverse elastic properties of chiral honeycombs*, Compos. Sci. Technol., **70,** 1057-1063.
26. Megson, T. H. G. 2013. Chapter 22 - Fuselages. *In:* MEGSON, T. H. G. (ed.) *Aircraft Structures for Engineering Students (Fifth Edition)*. Boston: Butterworth-Heinemann.
27. Mousanezhad, D., Haghpanah, B., Ghosh, R., Hamouda, A. M., Nayeb-Hashemi, H., Vaziri, A., (2016). *Elastic properties of chiral, anti-chiral, and hierarchical honeycombs: a simple energy-based approach*, Theor. Appl. Mech. Lett., **6,** 81-96.
28. Nečemer, B., Glodež, S., Novak, N., Kramberger, J., (2020). *Numerical modelling of a chiral auxetic cellular structure under multiaxial loading conditions*, Theor. Appl. Mech. Lett., 107**,** 102514.
29. Novak, N., Krstulović-Opara, L., Ren, Z., Vesenjak, M., (2020). *Compression and shear behaviour of graded chiral auxetic structures*, Mech. Mater., **148,** 103524.
30. Pan, S.-D., Wu, L.-Z., Sun, Y.-G., Zhou, Z.-G., Qu, J.-L., (2006). *Longitudinal shear strength and failure process of honeycomb cores*, Compos. Struct., **72,** 42-46.
31. Singh, J. P., Pandey, P. M., (2015). *Experimental investigations and statistical analysis of regular open cell porous metallic structure fabricated through rapid manufacturing*, Int. J. Mater. Eng. Innovation, **6,** 91-107.
32. Sugimura, Y., (2004). *Mechanical response of single-layer tetrahedral trusses under shear loading*, Mech. Mater., **36,** 715-721.

Received: February 09, 2022 / Accepted: June 15, 2022 / Paper available online: June 20, 2022 © International Journal of Modern Manufacturing Technologies